

Correlation between multiple ionization and fragmentation of C_2H_6 in charge-changing collisions with 580-keV C^+

T. Majima,^{1,2} T. Murai,² T. Kishimoto,² Y. Adachi,² S. O. Yoshida,² H. Tsuchida,^{1,2} and A. Itoh^{1,2}

¹*Quantum Science and Engineering Center, Kyoto University, Uji 611-0011, Japan*

²*Department of Nuclear Engineering, Kyoto University, Kyoto 615-8540, Japan*

(Received 13 October 2014; published 17 December 2014)

We investigate correlations between multiple ionization and fragmentation processes of the ethane molecule in collisions with 580-keV C^+ ions under single-electron capture and loss conditions. Employing an electron counting technique, we directly obtain number distributions of ionized electrons, which correspond to distributions of multiple ionization probabilities of ethane. In addition, fragmentation patterns as a function of the charge state r of intermediate parent ions $C_2H_6^{r+*}$ are obtained from coincidence measurements between the time of flight of the product ions and the number of electrons emitted. Fragmentation patterns in the different charge-changing conditions reveal a crucial role of the internal excitation in the fragmentation processes. Also, we provide clear evidence of strong selectivity on the parent charge state for formation of the H_3^+ ion, which is exclusively generated through doubly charged parent ions $C_2H_6^{2+*}$.

DOI: [10.1103/PhysRevA.90.062711](https://doi.org/10.1103/PhysRevA.90.062711)

PACS number(s): 34.50.Gb, 34.70.+e, 82.30.Lp

I. INTRODUCTION

Ion-impact ionization of molecules followed by subsequent dissociation is the first-stage fundamental process in the course of ion-irradiation effects on living cells [1]. In particular, multiple-electron ionization becomes important in collisions of fast heavy ions of MeV energies because the amount of electronic energy deposition becomes large. Unstable multiply charged molecules formed transiently in such collisions generate easily a variety of fragment products and radicals which are known to act as a trigger for complicated physicochemical reactions in the medium. It is also known that secondary electrons of less than a few tens of eV play a significant role in radiation damage of DNA [1–3]. Hence, quantitative information about the probability of multiple ionization and the resulting fragmentation of multiply charged molecular ions is of great importance to achieve fundamental understanding of the underlying mechanisms of radiation effects in matter.

To date, a large number of studies of collision-induced ionization, excitation, and fragmentation of molecules have been performed for isolated gas-phase molecular targets. Owing to recent development of coincidence techniques, correlation between fragment ions can be studied in detail for small-size molecules consisting of a few atoms [4]. In those measurements, distributions of multiple ionization are derived by summing up the charge states of the fragment ions detected together in each collision event [5,6]. As for larger molecules composed by many atoms, however, probabilities of the complete detection of several fragment ions becomes extremely low due to finite detection efficiency, limiting the possibility of determining the degree of multiple ionization of parent molecules formed transiently before fragmentation. Actually, experimental investigations of molecules—hydrocarbon molecules, for instance—are limited only to measurements of fragment ions and not more [7–23]. Little is known about the details of fragmentation processes from highly charged large molecules.

On the contrary, an electron counting method using a semiconductor detector is capable of direct deducing of the degree of multiple ionization. The method was originally

developed to measure the number distributions of secondary electrons from a solid surface by ion impacts [24,25], and then applied to studies of fragmentation of isolated C_{60} molecules in the gas phase [26–29]. For gas-phase molecular targets, the number of secondary electrons n_e gives straightforwardly the degree of multiple ionization of the target molecules. Furthermore, by measuring simultaneously the time of flight (TOF) of fragment ions, correlation between charge states of parent ions prior to fragmentation and fragmentation patterns can be deduced correctly. It should be stressed again that this coincidence technique has a great advantage over conventional methods particularly for highly multiple ionization of large molecules because reliable estimation of the intermediate charge state becomes practically impossible with limited detection efficiency of product ions from highly charged large molecules. We can expect that detailed studies on fragmentation processes of large molecular ions as a function of their charge states will shed new light on the characteristic decay mechanisms of highly charged molecular ions.

In this paper, we employed this technique to investigate fragmentation processes of the ethane molecule (C_2H_6) bombarded by 580-keV C^+ ions. It should be noted that this energy range and the charge state are more closely relevant to interaction in the Bragg peak region, compared to frequently investigated conditions like few keV or higher charge states [30–32]. We measured the distribution of multiple ionization of C_2H_6 molecules and the correlation between fragment ions and charge states of their parent ions. The measurements were performed under conditions of single-electron ($1e$) capture and loss collisions. It is noted that the fragmentation of ethane has been studied previously by means of conventional coincidence methods using electron impacts [33–36] and strong laser fields [37–42]. In particular, the H_3^+ production from hydrocarbon molecules has been known since early work in mass spectrometry [43] and still attracts considerable attention as one of the simplest examples of chemical reactions involving intramolecular bond rearrangement [7,12,38,39,42,44,45] and in interstellar chemistry [46]. In electron impacts and photoionization experiments, the H_3^+ ions are observed in binary fragmentation of

doubly charged parent ions, i.e., $C_2H_6^{2+} \rightarrow H_3^+ + C_2H_3^+$, using conventional coincidence methods [38–41,43]. Here, we examine more systematically the relationship between the charge state r and the H_3^+ production in the present ion-impact experiments in which parent molecules can be highly ionized with $r > 2$. In the following section, an outline of our experimental apparatus and method is described. In Sec. III, detailed discussion is given for fragment ion distributions in TOF spectra, secondary electron distributions equivalent to the distribution of multiple ionization, and correlation between fragment ions and charge states of their parent ions. Conclusions are given in Sec. IV.

II. EXPERIMENT

The experiment was performed at a 1.7-MV tandem accelerator facility of Quantum Science and Engineering Center, Kyoto University. Figure 1 shows a schematic diagram of the experimental setup consisting of our previous two different detection systems for secondary electrons using a solid-state detector [28,29] and for product ions using a position-sensitive detector [47]. A beam of 580-keV C^+ ions was collimated with two sets of four-jaw slits, then charge purified by a magnetic charge selector just before a collision chamber, and crossed with a gas jet target of C_2H_6 . A typical gas pressure in the collision chamber during measurements was about 6×10^{-4} Pa. Note that the velocity of the projectile ions is 1.4 a.u., at which an interaction with a target molecule is completed in the order of 0.1 fs.

Product ions, including fragment ions and intact ions of C_2H_6 molecules generated in collisions, were extracted perpendicular to the projectile-beam axis by an electric field with two mesh electrodes separated by 10 mm from each other. Ions were detected by a microchannel plate (MCP) detector in conjunction with a position-sensitive delay line detector (DLD). The total detection efficiency is limited by transmission probabilities of grid meshes of the extract electrodes and efficiency at the MCP detector and DLD. The detection probability of each product ion was estimated to be about 0.2 in the present system. The mass-to-charge ratio m/q of product ions was obtained with a TOF spectrometer operated under a Wiley-McLaren spatial focusing condition [48]. Pulse signals from the DLD were recorded with a digital storage oscilloscope (LeCroy, WavePro7000). The TOF and

the incident position on the MCP detector of each product ion were obtained by analyzing the timing of the pulse signals.

Outgoing projectile ions with different charge states q_f were separated by an electrostatic deflector and detected by a movable semiconductor detector (SSD_p). In this work, two charge-changing collision conditions corresponding to $1e$ capture ($q_f = 0$) and $1e$ loss ($q_f = 2$) were selected. Collision events occurring under a specific charge-changing condition were obtained from SSD_p signals as the trigger timing for the TOF measurements.

Secondary electrons emitted in collisions were extracted to the opposite direction of the product ions and detected by a semiconductor detector (SSD_e) on a potential at +25 kV. Each electron hits the detector with an energy of 25 keV, and thus the total energy of $25n_e$ keV is deposited into the SSD_e when n_e electrons are emitted in a single collision. Since the semiconductor detector provides signals with pulse heights proportional to the deposited energy, distributions of n_e are derived by analyzing pulse-height distributions (or energy spectra) of SSD_e signals. The pulse height of the SSD_e signal was recorded by a multichannel analyzer (MCA) in coincidence with the DLD signals of the product ions for each collision event. When no electron is detected during the gate of the MCA opening in coincidence with ion detection, the MCA records an amplitude of an electric signal fluctuating around the zero-volt baseline. Coincidence measurements between the TOF of ions and the pulse height of SSD_e signals provide information on correlation between fragment ions and the charge state of parent ions prior to fragmentation.

To deduce the number distributions correctly, the n_e spectra need to be analyzed by a fitting procedure based on the model which takes account of the electron loss due to finite collection efficiency and the electron backscattering at the detector surface [24]. Parameters used in the fitting procedure, including collection efficiency of the secondary electrons and so on, were evaluated from a separate experiment using an argon gas target. When an Ar^{r+} ion is detected in a $1e$ capture collision, the true number of n_e is uniquely determined to be $(r - 1)$ since one electron among r electrons is transferred to the projectile ion. By analyzing n_e distributions in coincidence with Ar^{r+} ($r = 1-4$) detections, the collection efficiency was estimated to be about 93%, which is consistent with the transmission rate of the mesh electrode. The other parameters used in the present analysis are basically similar to the previous values evaluated with the C_{60} target [28,29].

III. RESULTS AND DISCUSSION

Figure 2 represents two-dimensional (2D) coincidence maps between product ions and secondary electrons obtained for $1e$ capture and $1e$ loss collisions of 580-keV C^+ ions with C_2H_6 . The horizontal and vertical axes are the TOF of product ions and the pulse height of SSD_e signals, respectively. The pulse-height distributions are referred to as “ n_e spectra” hereafter. As shown in the figure, projection of the coincidence data in 2D maps onto the two axes gives a total TOF spectrum and a total n_e spectrum, respectively. Longitudinally aligned data points of n_e correlated with a specific product ion give the number of electrons emitted in collisions where the specific ion is produced, referred to as a “partial n_e spectrum” in this

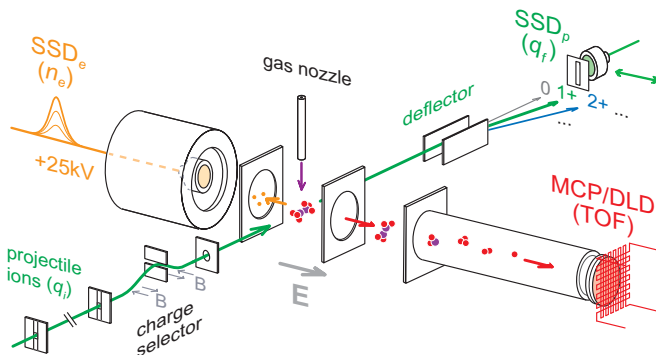


FIG. 1. (Color online) Schematic diagram of experimental setup.

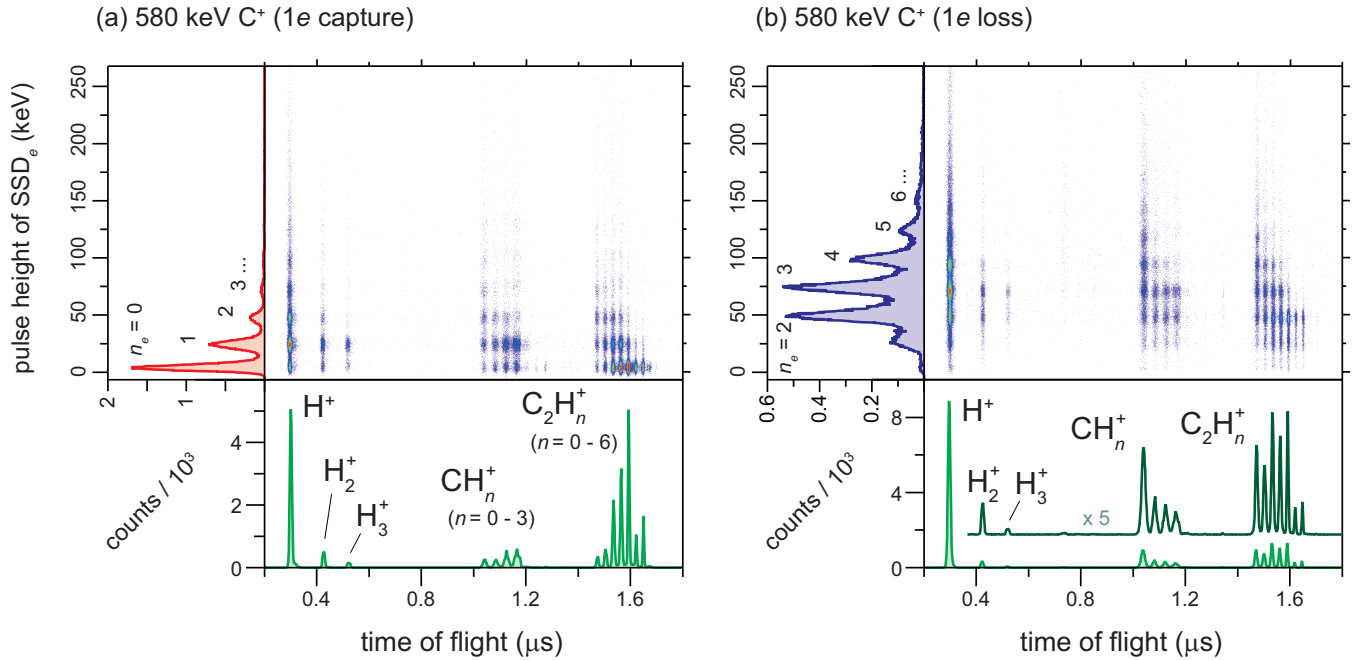


FIG. 2. (Color online) Two-dimensional coincidence maps between TOF of product ions and n_e from C_2H_6 molecules induced by collisions of 580-keV C^+ ions in the (a) $1e$ capture and (b) $1e$ loss conditions.

paper. Similarly, horizontally aligned data points in a specific n_e region give a partial TOF spectrum for collision events with n_e -electron emission. These spectra were carefully analyzed by taking account of the electron counting loss and backscattering effect at the detector surface of SSD_e [28,29]. The correction procedure of these effects is described in the Sec. III C.

A. Product ions (total TOF spectra)

The total TOF spectra of product ions are classified into three groups according to the number of constituent carbon atoms as follows: (i) ions which maintain a C-C bond, $C_2H_n^+$ ($n = 0-6$), (ii) ions with a single carbon atom, CH_n^+ ($n = 0-3$), and (iii) hydrogen atomic and molecular ions, H_n^+ ($n = 1-3$). In comparison with the electron-impact experiments [33–36], the present results show higher degrees of fragmentation achieved by large energy transfer induced by fast heavy ion collisions. Intensity distributions show that H^+ is the dominant product ion in both $1e$ capture and loss collisions. Besides H^+ , $C_2H_n^+$ ions of the group (i) are the second dominant products in both collisions, while C-C bond-broken ions of group (ii) are produced rather strongly in $1e$ loss collisions. Note that doubly charged $C_2H_{2n}^{2+}$ ions appear at the same TOF positions of singly charged CH_n^+ ions. Separation of these spectra is possible because of a large difference of peak widths due to different kinetic energies [40]. Namely, sharp peaks of $C_2H_{2n}^{2+}$ superimpose on broad peaks of C-C bond-broken CH_n^+ ions. Careful analysis of peak profiles reveals that the peak intensities of $C_2H_{2n}^{2+}$ ($n = 2, 3$) are about 10% of those of CH_n^+ ions in $1e$ capture collisions, while such double structures are not seen clearly in $1e$ loss collisions, indicating smaller fractions of the doubly charged ions.

A typical feature of TOF spectra in group (i) is that the $C_2H_4^+$ ion is produced most abundantly with intensities much

stronger than the intact parent ion $C_2H_6^+$ and $C_2H_5^+$ in both charge-changing collisions. The reason is explained by different appearance energies (E_{app}) of these ions. According to an experimental study with electron-impact ionization [49], the E_{app} of $C_2H_6^+$, $C_2H_5^+ + H$, and $C_2H_4^+ + H_2$ are 11.46, 12.7, and 11.90 eV, respectively. Namely, the difference of $E_{app}(C_2H_6^+)$ and $E_{app}(C_2H_4^+ + H_2)$ is only 0.44 eV, which basically corresponds to the energy barrier for dissociation into $C_2H_4^+ + H_2$. Thus, excited parent ions $C_2H_6^{*+}$, produced initially in collisions, can easily dissociate into $C_2H_4^+$ ions by releasing a neutral H_2 molecule as a result of relaxation of internal excitation energies deposited in collisions. In addition, $E_{app}(C_2H_5^+ + H)$ is higher than $E_{app}(C_2H_4^+ + H_2)$ by about 0.8 eV. Thus, $C_2H_6^+$ decays to $C_2H_4^+ + H_2$ as a preferential pathway rather than to $C_2H_5^+ + H$.

One can see that the intensity of CH_n^+ ions produced via C-C bond breakings are much stronger in $1e$ loss than $1e$ capture collisions. Also, the fragment ions with smaller number of hydrogen atoms n become stronger in $1e$ loss collisions; see, e.g., the C^+ ion as the dominant product ion in group (ii). These features imply evidently higher energy deposition in electron loss collisions than in capture collisions, reflecting the fact that electron loss occurs predominantly at smaller impact parameters while electron capture can take place even in distant collisions. Discussion is given in more detail in the following subsections.

B. Multiple ionization (total n_e spectra)

In Fig. 2, the n_e spectra (i.e., pulse-height distributions of SSD_e signals) show a series of separated peaks with a constant interval corresponding to 25 keV. Simultaneous detection of n_e electrons generates a pulse signal with a height corresponding to $25n_e$ keV. A peak as “ $n_e = 0$ ” around 0 keV

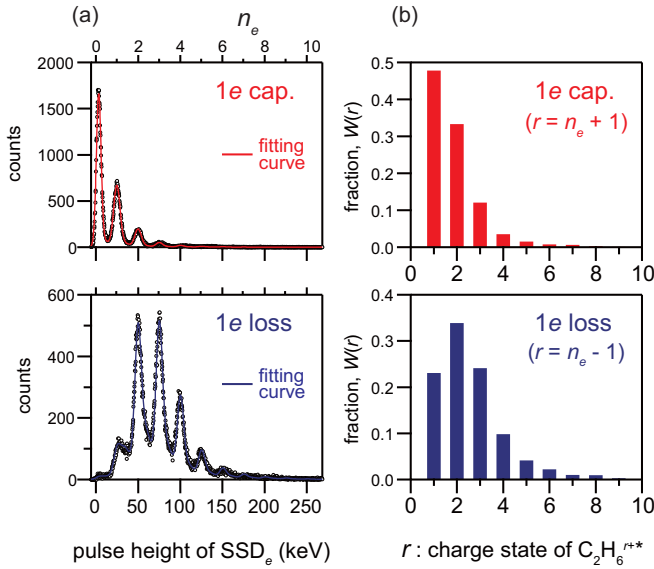


FIG. 3. (Color online) (a) Total n_e spectra and fitting curves for the 1e capture and 1e loss conditions; (b) distributions of charge state of $C_2H_6^{r+*}$ transiently generated via multiple ionization (and electron capture) in collisions with 580-keV C^+ ions.

in the 1e capture condition is due to pure single-electron capture collisions without additional ionization. The width of this peak reflects fluctuation of the baseline mainly due to thermal noise of the semiconductor detector. As observed clearly in the figure, such events of $n_e = 0$ are dominant and other peaks decrease steeply with increasing n_e in 1e capture collisions. In 1e loss collisions, the n_e distribution appears to take a maximum around $n_e = 2$ or 3. Figure 3(a) shows our fitting results by solid lines which reproduce perfectly the experimental n_e spectra (black dots) in both electron capture and loss collisions. Histograms depicted in Fig. 3(b) are the true number distributions deduced by this fitting procedure. Here, the data are plotted as a function of the charge state r of parent ions $C_2H_6^{r+*}$.

In our collision system, a target molecule C_2H_6 is highly ionized and excited transiently to unstable intermediate states and decays via subsequent fragmentation. Here, we define n_i as the number of “pure ionization” in which n_i electrons of a C_2H_6 molecule are released into vacuum without being captured by projectile ions. In terms of n_i and n_e , the values of r can be expressed as $r = n_i + 1 = n_e + 1$ for 1e capture ($n_e = n_i$) and $r = n_i = n_e - 1$ in 1e loss collisions ($n_e = n_i + 1$), respectively. Note that the lost electron from a projectile ion is also detected as one of the n_e electrons. The r distributions, cited as $W(r)$, represent distributions of the multiple ionization of the molecule. As can be seen in Fig. 3(b), nearly half of the events in 1e capture collisions arise from pure electron capture without additional ionization ($n_i = 0$ and $r = 1$), forming singly charged parent ions $C_2H_6^{+*}$. The relative probabilities of additional pure ionization of $n_i = 1$ and 2 (i.e., $r = 2$ and 3) are found to be about 0.3 and 0.1, respectively. On the contrary, multiple ionization is induced more intensively in 1e loss collisions. The distribution $W(r)$ reveals a maximum at double ionization ($n_i = r = 2$) and extends to $n_i \sim 6$ with sufficient intensities. The mean value of n_i is obtained as

2.6 while it is only 0.8 for 1e capture collisions. Higher multiple ionization in 1e loss collisions is consistent with higher multifragmentation discussed in Sec. III A.

Before proceeding to the discussion of correlation between multiple ionization and fragmentation, we emphasize again that the simultaneous measurement of the number of secondary electrons is essential (indispensable) to determine r distributions accurately. As mentioned before, for small molecular targets with a few constituent atoms, the charge state r may be deduced solely from coincidence data of product ions without knowing the number of secondary electrons. This is because the fragmentation of such a molecule involves only a few fragment ions at a maximum and all of them may be detected with a reasonably high probability. However, for larger molecules, the simultaneous detection of all the fragment ions becomes very hard due to limited detection efficiency of the ion detector. In the present measurement, the detected coincidence count of more than three ions was only a few out of 100 000 collision events recorded in each charge-changing condition. In such situations, it is impossible to deduce realistic distributions shown in Fig. 3(b), from the coincidence data of product ions.

C. Correlation between product ions and multiple ionization (TOF- n_e coincidence)

A series of r distributions of intermediate parent ions $C_2H_6^{r+*}$ correlated with specific product ions (labeled by i) were obtained accurately by analyzing the vertically aligned partial n_e spectra (Fig. 2), denoted by $W_i(r)$, hereafter. Figure 4 shows $W_i(r)$ for individual ions of CH_n^+ and $C_2H_n^+$ obtained in the 1e capture [red (light gray) bars] and loss [blue (dark gray) bars] conditions. A tiny fraction seen at $r = 2$ in $C_2H_6^+$ (right and bottom) is attributed either to fitting errors or accidental detection of stray electrons, because $W_i(r)$ must be unity at $r = 1$. It is found that $C_2H_5^+$ and $C_2H_4^+$ ions are produced predominantly from $C_2H_6^+(r = 1)$ via detachment of neutral H and H_2 , respectively. Contribution from doubly and more highly charged parent ions ($r \geq 2$) starts to appear for $C_2H_3^+$ and smaller ions. The $W_i(r)$ distributions of C_2H^+ and C_2^+ spread rather broadly around $r = 2$ and 3, respectively. As for CH_n^+ ($n = 1-3$) ions, the prominent correlation with $r = 2$ and more is found, implying that the C-C bond breaking primarily originates from multiply ionized states of $r \geq 2$. Note there is about 10% mixing of $C_2H_{6,4}^{2+}$ with $CH_{3,2}^+$ at $r = 2$. One can see clearly that the fraction of higher r increases with decreasing size n in CH_n^+ . Production of C^+ ions is most probable at $r = 2$ or 3 and extends up to $r \sim 6$.

Figure 5 shows partial n_e spectra and corresponding $W_i(r)$ distributions for H_n^+ ($n = 1-3$) ions. As expected, it is clearly shown that atomic hydrogen ions H^+ are generated from $C_2H_6^{r+*}$ with various charge states r . On the other hand, H_2^+ and H_3^+ ions are produced predominantly from doubly charged parent ions. In particular, the H_3^+ production is exclusively correlated with $C_2H_6^{2+*}$ and higher charge-state parent ions almost never generate H_3^+ ions. It is reported that H_3^+ ions are produced via binary fragmentation of doubly charged parent ions $C_2H_6^{2+} \rightarrow H_3^+ + C_2H_3^+$ in electron impacts and photoionization experiments [38–41,43]. Since these experiments have been done by conventional coincidence

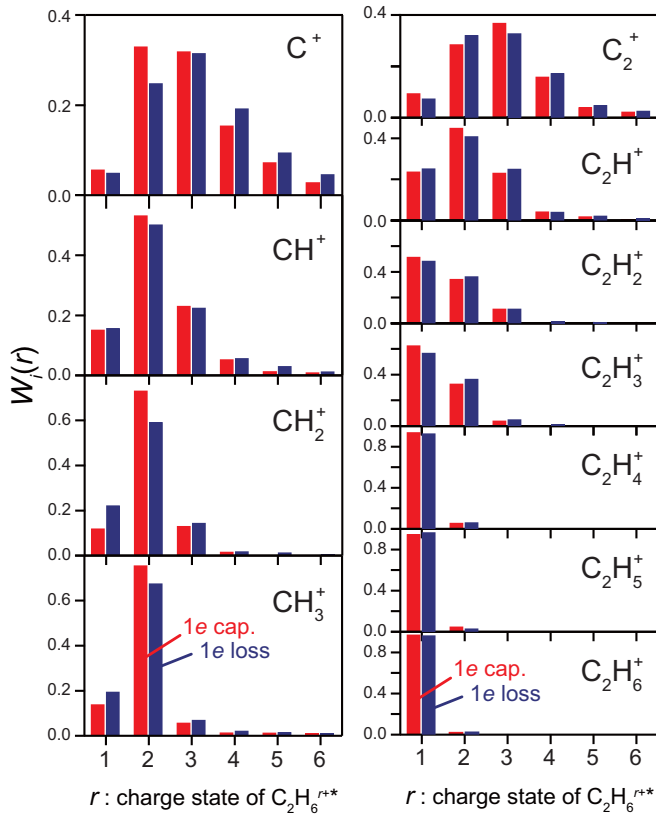


FIG. 4. (Color online) Charge-state distributions of intermediate parent ions $C_2H_6^{r+*}$ which lead to CH_n^+ and $C_2H_n^+$ productions in the $1e$ capture and $1e$ loss conditions.

methods, we stress here that this strong charge selectivity of H_3^+ formation pathway from $C_2H_6^{2+}$ is proved quantitatively in the present work. Correlation data among product ions reveal that H_3^+ ions are produced together with $C_2H_3^+$ and $C_2H_2^+$ ions, being consistent with previous photoionization experiments [43]. The branching ratio of pathways from $C_2H_6^{2+*}$ to either $H_3^+ + C_2H_3^+$ or $H_3^+ + C_2H_2^+ (+H)$ is obtained as 8:2 for both $1e$ capture and loss conditions. This branching ratio is nearly equivalent to the photoionization result of 85:15 reported in [43]. It means that the probability of neutral H emission accompanying the H_3^+ formation is less dependent on the ionization mechanisms. This is somewhat amazing because internal excited states of $C_2H_6^{2+*}$ are expected to be largely different from one another in $1e$ capture, $1e$ loss, and photoionization. Nevertheless, the almost equivalent branching ratios between ion impact and photoionization imply that the H_3^+ ion is generated only from specific excited states of $C_2H_6^{2+*}$ irrespective of the means of ionization.

Likewise, the r -distribution peaking at $r = 2$ for H_2^+ production indicates obviously that H_2^+ may also be produced predominantly through a preferential reaction pathway from doubly charged parent ions. An open question is the origin of this preferential charge selectivity of $r = 2$, unlike other fragment ion species although parent molecules are ionized widely from singly up to $r \sim 6$.

In order to demonstrate more explicitly the difference between $1e$ capture and loss collisions, the fragmentation

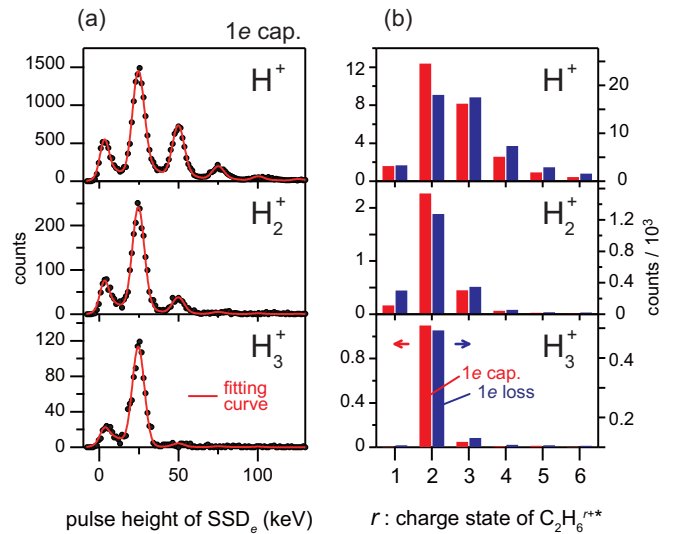


FIG. 5. (Color online) (a) Experimental results and fitting curves of partial n_e spectra for H_n^+ fragment ions ($n = 1-3$) generated in the $1e$ capture condition, (b) distributions of charge state r of intermediate parent ions $C_2H_6^{r+*}$ correlated with the H_n^+ productions, obtained as results of fitting procedure for the $1e$ capture and loss conditions.

patterns at fixed values of r are plotted in Figs. 6(a) and 6(b), where we plotted the intensities $I_r(i)$ of ions denoted by i from fixed charge states r of intermediate parent ions $C_2H_6^{r+}$,

$$I_r(i) = W_i(r)I(i), \quad (1)$$

where $I(i)$ is the total intensity of the product ion i derived from the total TOF spectra shown in Fig. 2. For comparison, distributions of fragment ions produced by 200-eV electron impacts [33] via $C_2H_6^{+*}$ and $C_2H_6^{2+*}$ parents are also shown as $r = 1$ and 2, respectively, in Fig. 6(c). It should be noted that these distributions were obtained by analyzing coincidence data of fragment ions without electron counting measurements. This is available for the electron-impact experiments because multiple ionization is less important in their experiment; double ionization is only 8% and triple ionization is negligibly small in total ionization.

Firstly, the $I_r(i)$ distribution at $r = 1$ in $1e$ capture conditions, as shown in Fig. 6(a) corresponding to the pure $1e$ capture process without additional ionization, shows $C_2H_n^+$ as the dominant product ion. It implies that the detachment of neutral H and/or H_2 is the main dissociation pathway from $C_2H_6^{+*}$. At $r = 2$, $C_2H_n^+$ ions are suppressed strongly while fragment ions of CH_n^+ and H_n^+ get produced prominently. Here, it is interesting to point out that the intensity distributions at $r = 1$ and 2 for $1e$ capture conditions surprisingly resemble those in Fig. 6(c) obtained by electron impacts [33]. This means that electronic excitation accompanied by $1e$ capture collisions is comparable to those with electron-impact ionization. Obviously, such gentle electron capture collisions correspond mainly to distant collisions.

With increasing charge state r , the bond-breaking processes proceed further. The intensity distributions of fragment ions with different n among CH_n^+ ($n = 0-3$) and $C_2H_n^+$ ($n = 0-6$) exhibit large shift toward smaller n with increasing r , resulting in the predominant production of H^+ , C^+ , and C_2^+ . In

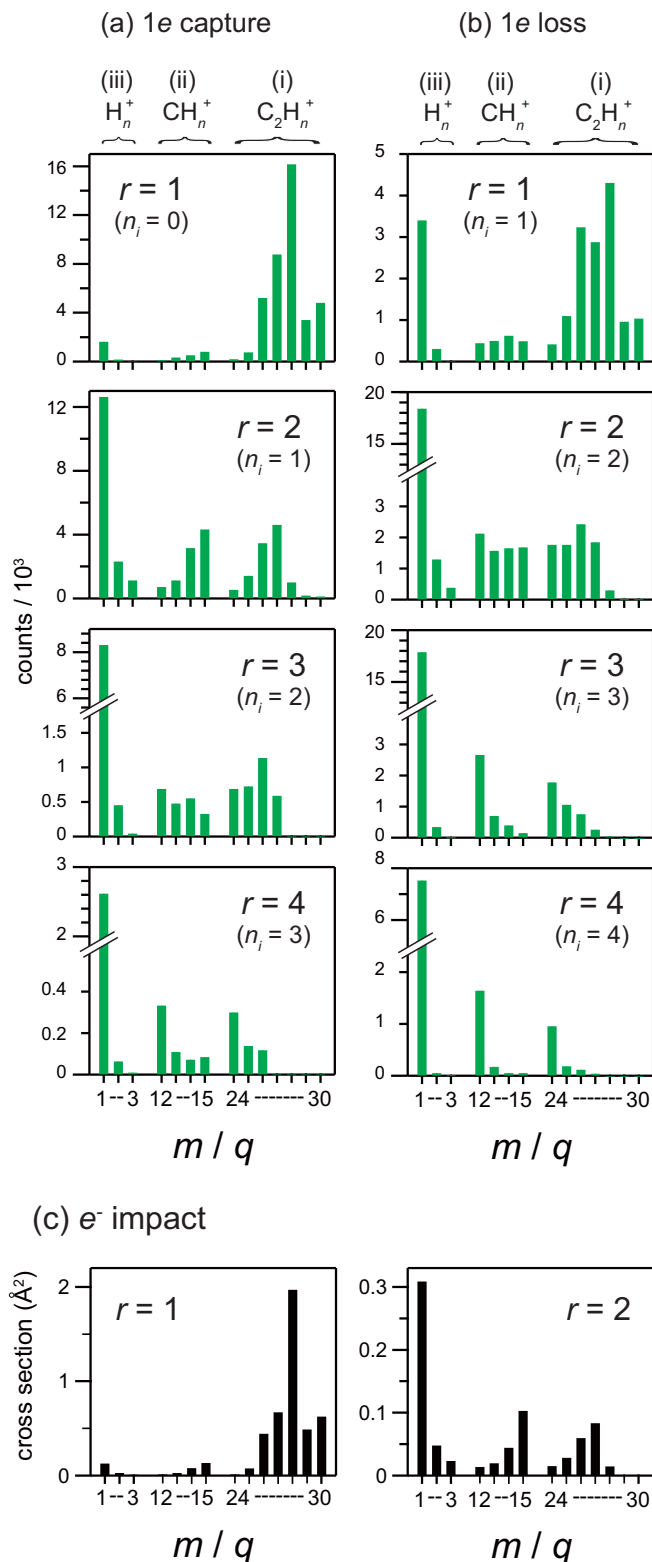


FIG. 6. (Color online) Intensity distributions of fragment ions as a function of the charge states r of parent ions $C_2H_6^{r++}$ in (a) $1e$ capture, (b) $1e$ loss collisions, and (c) 200-eV electron collisions [33].

contrast, we realize that the intensity ratio between groups (i) and (ii) does not change largely even at $r \sim 3$ and 4. In order to see this feature more explicitly, the intensities integrated over fragment ions in each group are plotted in Fig. 7 as a function

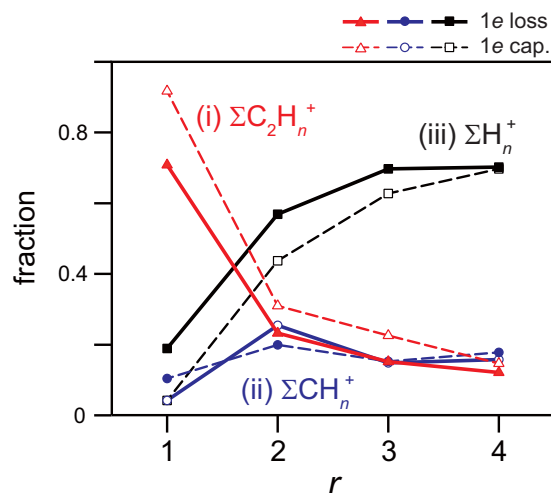


FIG. 7. (Color online) Fractions of integrated intensities of (i) $C_2H_n^+$ ($n=0-6$), (ii) CH_n^+ ($n=0-3$), and (iii) H_n^+ ($n=1-3$) in the total intensities of product ions as a function of the parent charge state r in the $1e$ capture and loss conditions.

of r . The integrated intensities of CH_n^+ and $C_2H_n^+$ are nearly equal to each other and do not change greatly at $r > 2$, meaning that probabilities of C-C bond cleavage are less enhanced with the increase of r . These results reveal an interesting feature of fragmentation of highly charged ethane molecules; prompt proton desorption before C-C bond breaking may act as a buffer which makes the C-C bond survive even at high charge states r .

Next, we compare the intensity distributions $I_r(i)$ between $1e$ capture and loss conditions. We can see here an important role of the internal energy in determining fragmentation patterns. Smaller fragment ions produced from C-H and C-C bond breakings appear rather prominently in $1e$ capture collisions at any r in comparison with those in $1e$ loss collisions. This high fragmentation in loss collisions means that higher internal excitation is induced in loss collisions than capture collisions even at the same charge state r . Furthermore, one can notice immediately the nearly equivalent fragmentation patterns between $r=3, 4$ in $1e$ capture and $r=2, 3$ in $1e$ loss collisions; $I_{r+1}(i)^{cap} \approx I_r(i)^{loss}$. This reminds us of the relationships $n_i = r - 1$ and $n_i = r$ for $1e$ capture and loss collisions, respectively. Namely, the fragmentation patterns in $1e$ charge-changing collisions are nearly the same when the numbers of pure ionization n_i are the same irrespective of the different values of r . It implies that the internal excitation energy, rather than the charge state r , governs the degree of fragmentation. This can be understood in the following way. Following a statistical model [50], the value of n_i is a good measure of the amount of internal excitation energy because the total electronic energy deposition from a projectile ion is shared between ionization and internal excitation with certain partition rates, e.g., 80% for ionization and 20% for excitation at the present incident velocity [50,51]. In addition, it is considered that $1e$ capture itself by an incident ion does not accompany greatly the extra excitation of the residual electronic system of a target molecule. Thus, once n_i is the same, the internal excitation energy of the molecule is

expected to be the same order of magnitude irrespective of either electron capture or loss collisions, resulting in the equivalent fragmentation patterns. It should be pointed out that this remarkable feature of n_i , instead of r , was observed in C_{60} fragmentation experiments using 2-MeV Si^{2+} ions [28]. It is somewhat surprising that such a simple statistical property seems to hold not only for C_{60} but also for C_2H_6 composed of only eight atoms.

IV. SUMMARY

Multiple ionization and subsequent dissociation of $C_2H_6^{r++}$ produced by 580-keV C^+ impacts have been investigated by a comprehensive coincidence method. Namely, simultaneous measurements of fragment ions and secondary electrons produced from gas-phase C_2H_6 molecules were performed in coincidence with the final projectile charge states under $1e$ capture and $1e$ loss conditions. With this method, we could directly obtain the multiple ionization probabilities in the specific charge-changing conditions. Consequently, we achieved detailed investigation of the fragmentation of highly charged molecules with specific charge states. Results obtained in this work are as follows.

The mean numbers of additional pure ionization n_i accompanying $1e$ capture and loss collisions were obtained as 0.8 and 2.6, respectively. Fragmentation patterns in total TOF spectra indicate higher energy deposition in $1e$ loss than $1e$ capture collisions, implying smaller impact-parameter collisions in $1e$ loss collisions. Comparison of partial TOF

spectra at fixed charge states r also exhibits a higher degree of multifragmentation in $1e$ loss than $1e$ capture collisions. However, if we compare the spectra at the same number of n_i both spectra are found to coincide fairly well with each other. This fact implies evidently from statistical arguments that the internal energy plays a decisive role for determination of the fragmentation patterns of ethane. We found that the C-C bond survives at a certain probability even in highly multiple ionization up to $r \sim 5$ or 6, indicating that the C-C bond in highly charged $C_2H_6^{r++}$ ions can remain until the ions become a singly charged state via prompt desorption of protons. Finally, we proved quantitatively that H_3^+ ions are generated only from specific excited states of doubly charged parent ions.

As demonstrated in this work for ethane molecules, the present coincidence technique is a promising powerful tool to make detailed investigation of multiple ionization of larger molecules such as biomolecules. Multiple ionization and charge-specific reaction processes of highly charged polyatomic molecular ions will be studied in detail in the future.

ACKNOWLEDGMENTS

The work was supported by JSPS KAKENHI Grants No. 24340096 and No. 23760826. One of the authors (T.M.) also would like to acknowledge the support by Mizuho Foundation for the Promotion of Sciences. We also acknowledge M. Naito for his technical support during the experiment.

-
- [1] *Radiation Damage in Biomolecular Systems*, edited by G. García Gómez-Tejedor and M. C. Fuss (Springer, Netherlands, Dordrecht, 2012).
- [2] P. Swiderek, *Angew. Chem., Int. Ed. Engl.* **45**, 4056 (2006).
- [3] B. Boudaïffa, P. Cloutier, D. Hunting, M. A. Huels, and L. Sanche, *Science* **287**, 1658 (2000).
- [4] D. Mathur, *Phys. Rep.* **391**, 1 (2004).
- [5] G. H. Olivera, C. Caraby, P. Jardin, A. Cassimi, L. Adoui, and B. Gervais, *Phys. Med. Biol.* **43**, 2347 (1998).
- [6] L. Adoui, C. Caraby, A. Cassimi, D. Lelièvre, J. P. Grandin, and A. Dubois, *J. Phys. B: At., Mol. Opt. Phys.* **32**, 631 (1999).
- [7] B. Jochim, A. Lueking, L. Doshier, S. Carey, E. Wells, E. Parke, M. Leonard, K. D. Carnes, and I. Ben-Itzhak, *J. Phys. B: At., Mol. Opt. Phys.* **42**, 091002 (2009).
- [8] I. Ben-Itzhak, K. D. Carnes, S. G. Ginther, D. T. Johnson, P. J. Norris, and O. L. Weaver, *Phys. Rev. A* **47**, 3748 (1993).
- [9] I. Ben-Itzhak, K. D. Carnes, D. T. Johnson, P. J. Norris, and O. L. Weaver, *Phys. Rev. A* **49**, 881 (1994).
- [10] U. Werner, B. Siegmann, H. Lebius, B. Huber, and H. O. Lutz, *Nucl. Instrum. Methods Phys. Res., Sect. B* **205**, 639 (2003).
- [11] B. Siegmann, U. Werner, and R. Mann, *Nucl. Instrum. Methods Phys. Res., Sect. B* **233**, 182 (2005).
- [12] S. De, J. Rajput, A. Roy, P. N. Ghosh, and C. P. Safvan, *Phys. Rev. Lett.* **97**, 213201 (2006).
- [13] S. De, J. Rajput, A. Roy, P. N. Ghosh, and C. P. Safvan, *Phys. Rev. A* **77**, 022708 (2008).
- [14] S. De, A. Roy, J. Rajput, P. N. Ghosh, and C. P. Safvan, *Int. J. Mass Spectrom.* **276**, 43 (2008).
- [15] V. V. Afrosimov, A. A. Basalaeov, Y. G. Morozov, M. N. Panov, O. V. Smirnov, and E. A. Tropp, *Tech. Phys.* **56**, 597 (2011).
- [16] D. Mathur and F. A. Rajgara, *J. Chem. Phys.* **124**, 194308 (2006).
- [17] K. Hayakawa, J. Mastumoto, H. Shiromaru, and Y. Achiba, *J. Phys. B: At., Mol. Opt. Phys.* **44**, 075207 (2011).
- [18] T. Mizuno, T. Yamada, H. Tsuchida, Y. Nakai, and A. Itoh, *J. Phys.: Conf. Ser.* **163**, 012039 (2009).
- [19] T. Mizuno and A. Itoh, *J. Phys.: Conf. Ser.* **488**, 012027 (2014).
- [20] A. I. S. Holm, H. Zettergren, H. A. B. Johansson, F. Seitz, S. Rosén, H. T. Schmidt, A. Ławicki, J. Rangama, P. Rousseau, M. Capron, R. Maisonnay, L. Adoui, A. Méry, B. Manil, B. A. Huber, and H. Cederquist, *Phys. Rev. Lett.* **105**, 213401 (2010).
- [21] A. Ławicki, A. I. S. Holm, P. Rousseau, M. Capron, R. Maisonnay, S. Maclot, F. Seitz, H. A. B. Johansson, S. Rosén, H. T. Schmidt, H. Zettergren, B. Manil, L. Adoui, H. Cederquist, and B. A. Huber, *Phys. Rev. A* **83**, 022704 (2011).
- [22] P. M. Mishra, J. Rajput, C. P. Safvan, S. Vig, and U. Kadhane, *Phys. Rev. A* **88**, 052707 (2013).
- [23] G. Reitsma, H. Zettergren, L. Boschman, E. Bodewits, R. Hoekstra, and T. Schlathölter, *J. Phys. B: At., Mol. Opt. Phys.* **46**, 245201 (2013).
- [24] G. Lakits, F. Aumayr, and H. Winter, *Rev. Sci. Instrum.* **60**, 3151 (1989).

- [25] A. Itoh, T. Majima, F. Obata, Y. Hamamoto, and A. Yogo, *Nucl. Instrum. Methods Phys. Res., Sect. B* **193**, 626 (2002).
- [26] L. Chen, J. Bernard, A. Denis, S. Martin, and J. Désesquelles, *Phys. Rev. A* **59**, 2827 (1999).
- [27] S. Martin, L. Chen, A. Denis, R. Bredy, J. Bernard, and J. Désesquelles, *Phys. Rev. A* **62**, 022707 (2000).
- [28] T. Majima, Y. Nakai, H. Tsuchida, and A. Itoh, *Phys. Rev. A* **69**, 031202 (2004).
- [29] T. Majima, Y. Nakai, T. Mizuno, H. Tsuchida, and A. Itoh, *Phys. Rev. A* **74**, 033201 (2006).
- [30] J. de Vries, R. Hoekstra, R. Morgenstern, and T. Schlathölter, *Phys. Rev. Lett.* **91**, 053401 (2003).
- [31] S. Martin, C. Ortega, L. Chen, R. Brédy, A. Vernier, P. Dugourd, R. Antoine, J. Bernard, G. Reitsma, O. Gonzalez-Magaña, R. Hoekstra, and T. Schlathölter, *Phys. Rev. A* **89**, 012707 (2014).
- [32] R. Brédy, J. M. Bernard, L. Chen, G. Montagne, B. Li, and S. Martin, *J. Chem. Phys.* **130**, 114305 (2009).
- [33] P. Wang and C. R. Vidal, *Chem. Phys.* **280**, 309 (2002).
- [34] C. Tian and C. R. Vidal, *J. Chem. Phys.* **109**, 1704 (1998).
- [35] J. A. Hipple, Jr., *Phys. Rev.* **53**, 530 (1938).
- [36] J. W. Au, G. Cooper, and C. E. Brion, *Chem. Phys.* **173**, 241 (1993).
- [37] S. Palaniyappan, R. Mitchell, N. Ekanayake, A. M. Watts, S. L. White, R. Sauer, L. E. Howard, M. Videtto, C. Mancuso, S. J. Wells, T. Stanev, B. L. Wen, M. F. Decamp, and B. C. Walker, *Phys. Rev. A* **82**, 043433 (2010).
- [38] P. M. Kraus, M. C. Schwarzer, N. Schirmel, G. Urbasch, G. Frenking, and K.-M. Weitzel, *J. Chem. Phys.* **134**, 114302 (2011).
- [39] K. Hoshina, Y. Furukawa, T. Okino, and K. Yamanouchi, *J. Chem. Phys.* **129**, 104302 (2008).
- [40] K. Hoshina, H. Kawamura, M. Tsuge, M. Tamiya, and M. Ishiguro, *J. Chem. Phys.* **134**, 064324 (2011).
- [41] R. Kanya, T. Kudou, N. Schirmel, S. Miura, K.-M. Weitzel, K. Hoshina, and K. Yamanouchi, *J. Chem. Phys.* **136**, 204309 (2012).
- [42] N. Schirmel, N. Reusch, P. Horsch, and K.-M. Weitzel, *Faraday Discuss.* **163**, 461 (2013).
- [43] J. H. D. Eland, *Rapid Commun. Mass Spectrom.* **10**, 1560 (1996).
- [44] K. Nakai, T. Kato, H. Kono, and K. Yamanouchi, *J. Chem. Phys.* **139**, 181103 (2013).
- [45] S. Bari, P. Sobocinski, J. Postma, F. Alvarado, R. Hoekstra, V. Bernigaud, B. Manil, J. Rangama, B. Huber, and T. Schlathölter, *J. Chem. Phys.* **128**, 074306 (2008).
- [46] T. Oka, *Faraday Discuss.* **150**, 9 (2011).
- [47] T. Mizuno, T. Yamada, H. Tsuchida, Y. Nakai, and A. Itoh, *Phys. Rev. A* **81**, 012704 (2010).
- [48] W. C. Wiley and I. H. McLaren, *Rev. Sci. Instrum.* **26**, 1150 (1955).
- [49] E. Vašková, M. Stano, Š. Matejíček, J. Skalný, P. Mach, J. Urban, and T. Märk, *Int. J. Mass Spectrom.* **235**, 155 (2004).
- [50] J. H. Miller and A. E. S. Green, *Radiat. Res.* **54**, 343 (1973).
- [51] H. Tsuchida, A. Itoh, K. Miyabe, Y. Bitoh, and N. Imanishi, *J. Phys. B: At., Mol. Opt. Phys.* **32**, 5289 (1999).